NJC

Accepted Manuscript

This article can be cited before page numbers have been issued, to do this please use: M. Bonomo, F. Sabuzi, A. Di Carlo, V. Conte, D. Dini and P. Galloni, *New J. Chem.*, 2017, DOI: 10.1039/C6NJ03466G.

ROYAL SOCIETY OF CHEMISTRY

rsc.li/njc

View Article Online
DOI: 10.1039/C6NJ03466G

Journal Name

ARTICLE

KuQuinones as sensitizers of NiO based *p*-type dye-sensitized solar cells

Received 00th January 20xx,
Accepted 00th January 20xx

DOI: 10.1039/x0xx00000x

www.rsc.org/

Matteo Bonomo,[a†] Federica Sabuzi,[b†] Aldo Di Carlo,[c] Valeria Conte,[b] Danilo Dini[a*] and Pierluca Galloni[b*]

A new series of KuQuinones (KuQs) has been synthesized and employed as dye-sensitizers of NiO-based *p*-type dye-sensitized solar cells (*p*-DSSCs). KuQs are pentacyclic quinoid compounds which are characterized by a fully conjugated structure that is responsible of the strong and broad absorption in the visible spectrum. The HOMO/LUMO states of the KuQs here considered match their energy levels with the upper edge of NiO valence band and I^-/I_3^- redox potential energy. These features render such compounds suitable for NiO sensitization in *p*-DSSC. The new carboxylic acid-substituted KuQs derivatives here proposed differ for the length of the alkyl chain. The *JV* characteristic curves and external quantum efficiency spectra have been recorded. Results showed that performances of KuQs-sensitized cells were similar to that of benchmark sensitizer erythrosine B (Ery B), despite the lack of electronic conjugation between the anchoring group and the light absorbing unit. This result led us to hypothesize that the photoinduced charge transfer between excited KuQs dyes and the NiO electrode occurred through space and not via chemical bonds as usually occurs in these systems. The mechanism of charge transfer through space has been supported by data of IR spectroscopy.

Introduction

p-type dye-sensitized solar cells (*p*-DSSCs) are photoelectrochemical devices that convert solar radiation into electrical power through a photoinduced process of redox reduction.[1-4] The most important feature related to the development of *p*-DSSCs is the nature itself of the photoactivated process, i.e. the electrochemical reduction of an appropriate species following the charge separation at the light absorbing cathode. In addition to the electrical power, a photoinduced reduction process can lead also to the formation of chemicals having a very strong economic and environmental impact, such as solar generated fuels (H_2 *in primis*),[5] as well as the products of direct CO_2 photo-transformation.[6-8] Currently, the highest reported efficiency for a NiO based *p*-DSSC is 2.5%.[9] Interestingly, *p*-DSSCs can be implemented as parts of tandem DSSCs (*t*-DSSCs), where both semiconducting electrodes are properly sensitized with dyes having complementary absorption features.[10-14] Theoretical conversion efficiencies up to 1.5 times larger than the respective DSSCs with single photoactive electrode can be obtained with *t*-DSSCs.[15] The most widely used photocathodic material for *p*-DSSCs is NiO (a *p*-type semiconductor) in the configuration of thin film (thickness < 3.5 μm)[16-20] with nanostructured features and wide bandgap (E_g > 3.2 *e*V).[21] The open morphology of mesoporous NiO films allows the anchoring of large amounts of dye (ca. 10^{-11} moles per cm^2 of electrode),[14] with consequent efficient sensitization of the *p*-DSSC photocathode. The working principle of a *p*-DSSC consists in the electron transfer (*ET*) from NiO cathode to the photoexcited dye-sensitizer with successive *ET* from the transiently reduced dye to the oxidized form of a redox shuttle (Fig. 1).[22] Beside the studies of NiO electrodes feasibility[23-26] and the investigation of alternative *p*-type semiconductors,[27,28] the research on *p*-DSSCs (and *t*-DSSCs) has also considered the preparation of novel organic dyes for progressively performing devices. Among these, the classes of erythrosines,[11,29] coumarines,[30-33] triphenylamines,[34,35] perylene imides,[13,18,36] isoindigo dyes,[37] squaraines,[38,39] porphyrins,[40] BODIPYs,[14,41] push–pull conjugated molecules,[42,43] diketopyrrolopyrroles,[44] and pyridyl metal complexes[45-47] have been explored for improving the effectiveness of hole photoinjection and for preventing recombination phenomena.[48] Moreover, recently Zhang and Cole investigated the use of different anchoring groups for *n*-type DSSC.[49] Nevertheless, as far as we are aware, just few examples of non-conjugated linkers for p-DSSC have been reported.[50] As an example, in 2007 Ooyama and co-workers developed some carbazole-based fluorescent dyes

[a] Dept. of Chemistry, University of Rome Sapienza, P.le A. Moro 5, 00185 Rome, Italy.
[b] Dept. of Chemical Sciences and Technologies, University of Rome Tor Vergata, Via della Ricerca Scientifica 1, 00133 Rome, Italy.
[c] Centre for Hybrid and Organic Solar Energy (CHOSE), Dept. of Electronic Engineering, University of Rome Tor Vergata, Via del Politecnico 1, 00133 Rome, Italy.
† These two authors contributed equally.
Email: galloni@scienze.uniroma2.it, danilo.dini@uniroma1.it
Electronic Supplementary Information (ESI) available: [details of any supplementary information available should be included here]. See DOI: 10.1039/x0xx00000x

View Article Online
DOI: 10.1039/C6NJ03466G

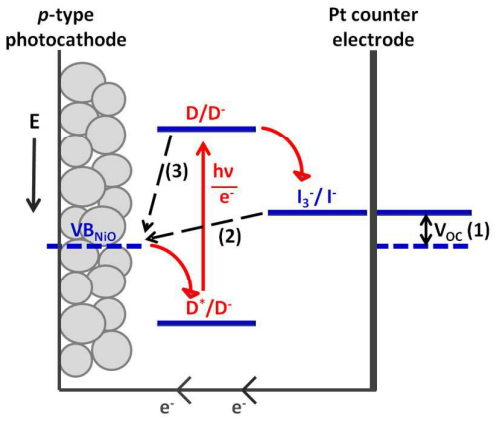

Fig. 1. Levels of the electrical potential, *E*, that participate in the photoinduced electron transfer process. Separation (1) indicates the width of the open circuit voltage V_{OC} for a NiO based *p*-DSSC. The redox couple I_3^-/I^- represents the redox mediator (or redox shuttle). In the scheme, the dye-sensitizer unit (D) absorbs light for the photoactivated electron transfer. Dotted arrows (2) and (3) show two possible processes of electronic recombination (unwanted phenomena) successive to the charge separation step induced by dye photoactivation.

and for the first time a through space *ET* has been suggested.[51] This result provided a new strategy for dyes-design: in fact, inspired by such approach Hao *et al.* synthesized a new class of D-p-A dyes (η = 3.7 %)[52] and quite recently, they reported the employment of similar dyes as sensitizers for NiO-based *p*-type DSSC.[53]

Here we report for the first time the adoption of a novel class of organic dyes, called KuQuinones (KuQs),[54] as sensitizers in *p*-type DSSCs. These compounds are able to harvest light in the visible region of the spectrum, due to their pentacyclic and totally conjugated structure, which makes them suitable dyes in solar-energy conversion devices.[55] In this work, properly substituted KuQuinones derivatives, which structures are reported in Fig. 2, have been synthesized, with the aim to anchor them on NiO electrodes. It is important to note how these KuQs employed non conjugated linkers as anchoring groups (Fig. 2).

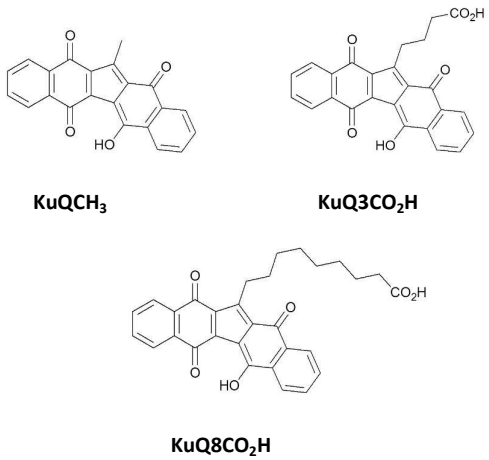

Fig. 2. Structures of the new KuQs employed as dye-sensitizers in this study.

Moreover, for the first time an alkyl chain longer than propyl (i.e. octyl) has been used as anchoring unit. The performances of KuQs photosensitizers of mesoporous NiO cathodes for *p*-DSSCs have been tested and compared with the one of the common benchmark sensitizer, EryB.[56]

Results and discussion

Synthesis and characterization of the dyes

The novel substituted KuQs derivatives have been synthesized following a procedure previously reported in the literature.[54] The general reaction requires 2-hydroxy-1,4-naphtoquinone as starting compound, which is dissolved in DMSO in the presence of an excess of an alkyl bromide, an inorganic base and a catalytic amount of ferrocene. The one-pot reaction leads to the formation of a pentacylcic, fully conjugated compound, where two molecules of the hydroxynaphtoquinone are condensed with one molecule of the alkyl bromide. Unexpectedly, the reaction proceeds with the loss of one carbon atom, apparently from the alkyl bromide; however, a full understanding of the mechanism is still not achieved. By changing the nature of the alkyl bromide, a small library of KuQuinone derivatives has been already synthesized: compounds differ in side chain length or functional group. In the perspective of employing KuQs as dye-sensitizers in *p*-type DSSC, the synthesis of KuQs with a carboxylic acid as terminal group bound on the alkyl side chain was mandatory in order to covalently link the organic dye to a metal oxide electrode. In this context, several attempts to obtain the desired compounds using carboxylic acid-functionalized alkylbromide (such as 6-bromohexanoic acid or 11-bromoundecanoid acid) as alkyl bromide source have been performed, but no products were obtained. Likely, in the reaction conditions adopted, the intra-molecular substitution reaction between the carboxylate group and the alkyl bromide portion occurs, making the reagent unsuitable for the reaction.[57] Alternatively, KuQs containing a carboxylic acid group could be easily obtained by hydrolysis of the corresponding esters (Scheme 1). Specifically, ethyl 6-bromohexanoate and ethyl 11-bromoundecanoate have been synthesized and subsequently used as reagents in KuQs synthesis, leading to 1-(3-ethoxycarbonylpropyl)KuQuinone ($KuQ3CO_2Et$) and 1-(8-ethoxycarbonyloctyl)KuQuinone ($KuQ8CO_2Et$), respectively. $KuQ3CO_2Et$ and $KuQ8CO_2Et$ have been obtained in good yields if compared with the other KuQs derivatives previously synthesized.[54] Moreover, the adopted purification procedures resulted much easier than the other, because of the formation of lower amounts of undesired side products.

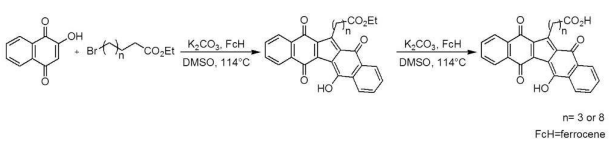

Scheme 1. Synthesis of KuQuinones

View Article Online
DOI: 10.1039/C6NJ03466G

Hydrolysis of the ester groups led to the formation of the corresponding carboxylic acids in very high yields.

$KuQ3CO_2H$ and $KuQ8CO_2H$ showed very low solubility in all conventional organic solvents, except in THF. UV-vis absorption spectra recorded in this solvent are reported in Fig. 3. They have been compared with the absorption spectrum of 1-methylKuQuinone ($KuQCH_3$) in toluene, which synthesis was previously reported.[54]

All the spectra were characterized by two intense bands between 420 and 600 nm with molar extinction coefficients up to 15000 $M^{-1}cm^{-1}$. Another absorption band with lower intensity, was detected between 350 and 400 nm; this band becomes much more intense upon deprotonation of enol oxygen.[55] The partial blue shift of the novel synthesized KuQs with respect to the absorption spectrum of $KuQCH_3$ is probably due to solvent properties, which can affect the spectral profiles of similar compounds.[57]

The energy levels of HOMO-LUMO orbitals have been determined with density functional theory (DFT) and B3LYP hybrid functional with 6-311G dp basis set.[59] HOMO and LUMO orbitals of KuQuinone dyes are shown in Fig. 4.

For all compounds, both HOMO and LUMO show electronic conjugation due to π-electrons. Specifically, HOMO-orbitals are centered in the middle region of the pentacyclic systems and they are extended up to the carbonyl groups, where the electronic density is much higher. Moreover, they are partially delocalized on the alkyl side chain. In this regard, the long C sp^3 chain in $KuQ8CO_2H$ does not allow the carboxylic acid group to electronically interact with the pentacyclic core. For this reason, the scheme of the energies of the frontier orbitals is very similar to that of $KuQCH_3$. In $KuQ3CO_2H$, the HOMO orbital is extended along the short alkyl side chain, up to the carboxylic acid, which can interact with the pentacyclic system thus lowering the orbital energy. Concerning the LUMO-level, these orbitals are distributed all over the π-system, showing a complete delocalization. The position of the LUMO level is not influenced by the side chain length and the presence of carboxylic acid group but it is exclusively dependent from the conjugated system.

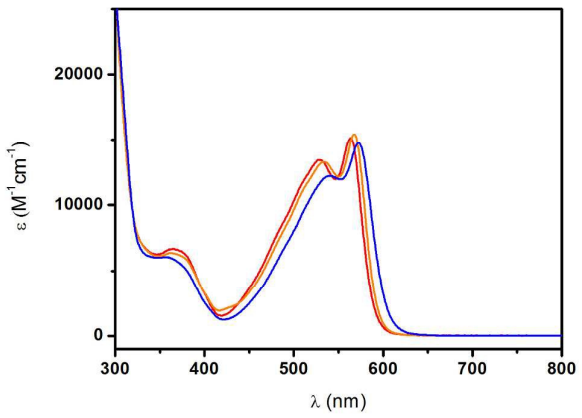

Fig. 3. UV-vis absorption spectrum of $KuQ3CO_2H$ (red line) and $KuQ8CO_2H$ (orange line) in THF and $KuQCH_3$ in toluene (blue line).

We outline here that $KuQ3CO_2H$ LUMO energy is slightly lower than that of $KuQCH_3$ and $KuQ8CO_2H$. This evidence is quite important for *p*-type DSSC: if the energy level of LUMO is positioned far from the upper edge of the valence band of the semiconductor, the undesired phenomenon of recombination is minimized, thus an energetically distant LUMO entails lower recombination rate.

The energy values of the HOMO-LUMO states calculated with DFT are reported in Table 1. An experimental confirmation of the validity of such theoretical results is given by cyclic voltammetries of these dyes dissolved in dichloromethane (see SI). Specifically, the energy level of LUMO has been calculated by measuring the reduction potential (E_{red}) of each dye, while the energy level of HOMO (that is higher than 2 V) has been estimated according to the following equations:[60]

$$E\ (HOMO) = E\ (LUMO) - E_g \qquad (1)$$

$$E_g = h\nu = \frac{hc}{\lambda} = \frac{1242}{\lambda_{onset}} \qquad (2)$$

where E_g corresponds to the optical energy gap that can be calculated through UV-visible spectroscopy, using λ_{onset} as the longest absorption wavelength.

For all compounds the energy values of HOMO and LUMO theoretically and experimentally calculated show a discrepancy comprised between 0.5 and 0.85 eV, as commonly observed for similar comparisons.[60a,c,61] Unlike the theoretical calculations - where HOMO and LUMO energies relative to $KuQ3CO_2H$ were slightly lower than those of $KuQCH_3$ and $KuQ8CO_2H$ - experimental data show comparable energies for all compounds.

All the KuQs derivatives here proposed have frontier orbitals with appropriate energy in relation to the position of the upper edge of NiO valence band and I^-/I_3^- redox energy level. This makes our compounds suitable for NiO sensitization and their consequent application as dyes in the corresponding *p*-DSSC.

Table 1. HOMO-LUMO energy levels for KuQs dyes.

	Theoretically calculated[a]		*Experimentally calculated*		
Dye	**HOMO (eV)**	**LUMO (eV)**	**E_g (eV)**	**HOMO (eV)**	**LUMO (eV)[b]**
$KuQ3CO_2H$	-6.61	-3.80	2.21	-6.60	-4.39
$KuQ8CO_2H$	-6.30	-3.52	2.19	-6.56	-4.37
$KuQCH_3$	-6.32	-3.50	2.17	-6.51	-4.34

[a] Frontier orbitals energy levels have been estimated through DFT calculations using B3LYP hybrid functional with 6-311G dp basis set; energies are referred to the *vacuum*.

[b] Values have been calculated using cyclic voltammetry conducted in a 0.1 M solution of TBAP in CH_2Cl_2 at a scan rate of 100 mV/s. A standard calomel electrode (SCE) was used as the reference electrode, a platinum wire as counter electrode and a platinum disk as working. Data in the table are referred to the NHE potential, set 4.44 eV below the *vacuum* level. Specifically, energy of LUMO level has been calculated using the following equation: $E_{LUMO} = -e\ [E_{red} + 4.4]$.[60]

View Article Online
DOI: 10.1039/C6NJ03466G

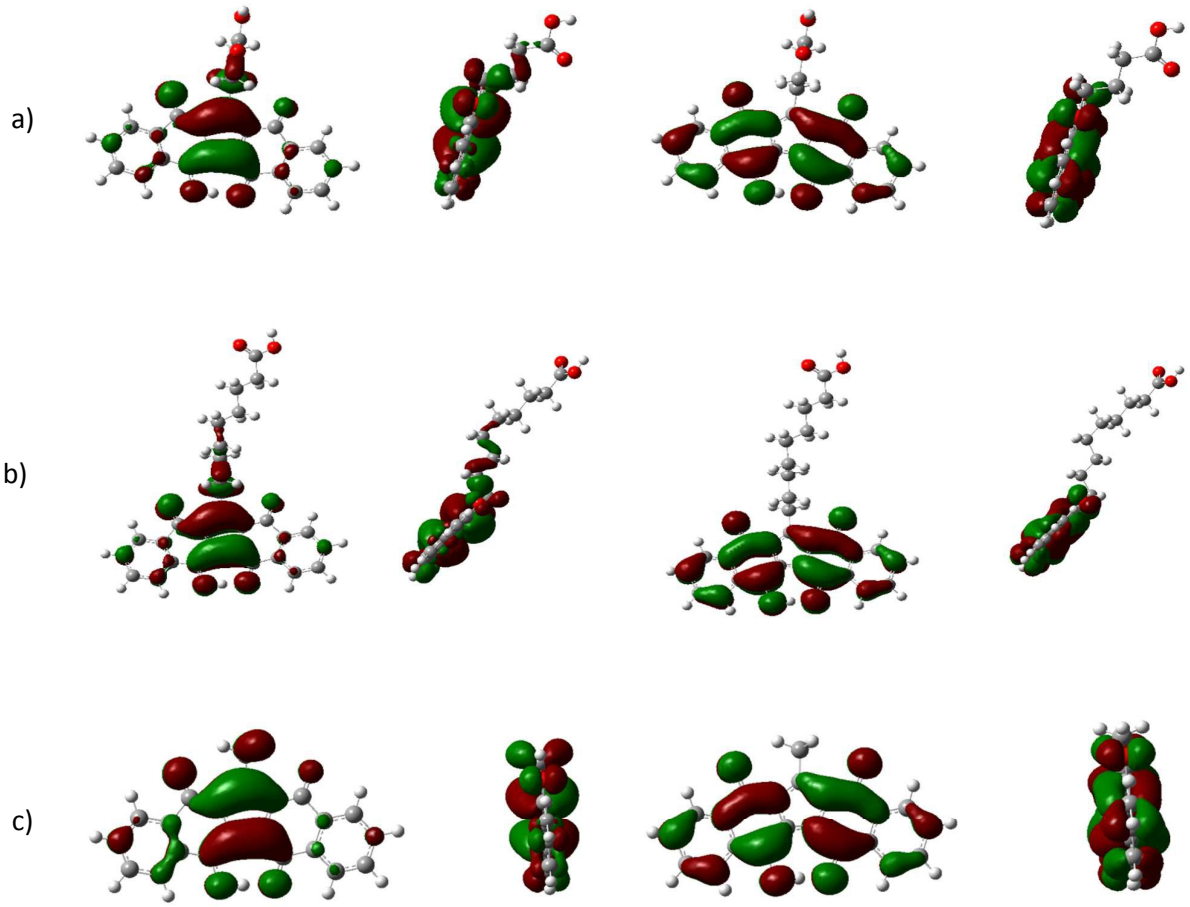

Fig. 4. Representation of HOMO (front and side view, on the left) and LUMO (front and side view, on the right) orbitals for $KuQ3CO_2H$ (a), $KuQ8CO_2H$ (b) and $KuQCH_3$ (c).

NiO characterization

NiO thin films have been prepared as deposits on a FTO-covered glass panel through screen-printed technique (see Experimental).

Screen-printed NiO presented an open and scale-like morphology with cavities and apertures having a linear size in the order of few hundreds of nanometers (Fig. 5).

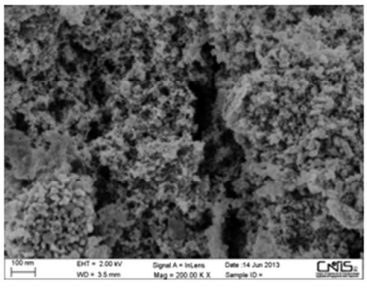

Fig. 5. SEM image of NiO electrode.

The presence of such voids in the NiO electrode surface ensures a high contact area between the sensitized layer of NiO and the liquid electrolyte throughout the whole thickness of the oxide film. Since NiO is an electroactive material, another important consequence of its nanoporosity is the direct proportionality between thickness and current exchanged by the electrode. The crystal structure, as well as the surface morphology and the electrical connectivity between nanostructured units affect the device behavior since they are all responsible of the charge transport between NiO and the supporting substrate.[62] Previous studies demonstrated that in NiO-based *p*-DSSC the optimum film thickness is approximatively 2,5 µm.[26]

NiO has been spectrophotometrically characterized before the assembly in the *p*-DSSC (Fig. 6). The transmittance of NiO in the visible spectrum was quite high, thus indicating the good transparency of the electrode. Subsequently, NiO electrodes were functionalized with the novel synthesized dyes in order to test their possible application in *p*-type DSSC. In general, optimal dyes need to be chemisorbed on the oxide surface in

View Article Online
DOI: 10.1039/C6NJ03466G

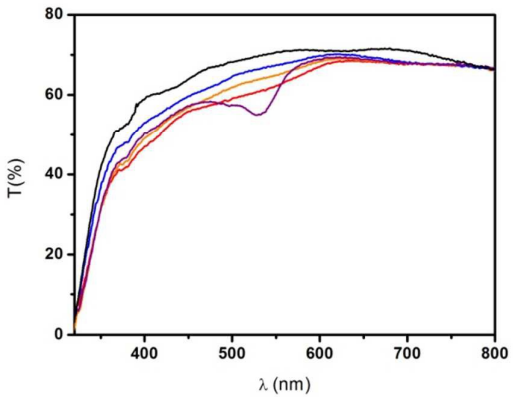

Fig. 6. Transmittance spectra of: non-functionalized NiO bare (black line), EryB-functionalized NiO (purple line), KuQ3CO$_2$H-functionalized NiO (red line), KuQ8CO$_2$H-functionalized NiO (orange line) and KuQCH3-functionalized NiO (blue line).

order to be strongly anchored on the oxide.

In this regard, KuQs derivatives having a carboxylic group on the side chain have been prepared (Fig. 2). Moreover, looking at the general structure of KuQuinones, it can be noticed that the enol group and the vicinal carbonyl oxygen are at the appropriate distance for coordinating transition metal ions, such as nickel ions on the electrode surface. This geometry of coordination allowed the binding of similar organic compounds, such as 4-hydroxyanthraquinone derivatives, to Ti^{4+} ions in TiO_2 electrodes, generating devices having energy conversion efficiencies up to 1.5%.[63] Likewise, the sensitization of NiO through the coordination of KuQs by nickel cations is expected, with the opportunity to bind also KuQCH$_3$ to the NiO electrode surface (Fig. 7). However, it can be observed that transmittance spectra of the KuQuinones adsorbed on NiO electrodes were only slightly different from the reference electrode (Fig. 6). In particular, if compared to the sharp, well defined peak obtained with EryB dye, KuQ3CO$_2$H and KuQ8CO$_2$H spectra showed a very broad peak in the region between 460 and 630 nm, which probably indicates the presence of aggregates. In fact, it is already known that the planar, pentacyclic and fully conjugated structure of KuQs may favor aggregation phenomena on electrode surfaces.[55] Conversely, transmittance spectrum of KuQCH$_3$ on NiO was comparable with the non-functionalized NiO, indicating that the expected coordination between KuQuinones and NiO through enol and carbonyl oxygen atoms did not occur. This evidence clearly makes the KuQCH$_3$ dye unsuitable for DSSC application. On the other hand this finding constitutes a further confirmation that the chemisorption of KuQ3CO$_2$H and KuQ8CO$_2$H occurs through the carboxylic group bound on the side chain (Fig. 8).

ATR-FTIR spectroscopy clearly confirmed the formation of such bond. In fact, IR spectra of pure KuQ3CO$_2$H and KuQ8CO$_2$H show a well defined peak respectively at 1708 and 1695 cm^{-1}, which are ascribable to the C=O stretching peak in the carboxylic acid group (see Supp. Info). Once adsorbed on NiO such signal totally disappear. This experimental evidence unambiguously indicates that the bond between NiO surface and KuQs occurs through the carboxylic anchoring group[53,64] (Fig. 9), thus confirming the bidentate bridging structure reported in Fig. 8.[64]

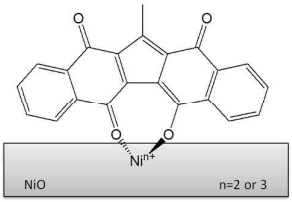

Fig. 7. Expected KuQCH$_3$ coordination to NiO.

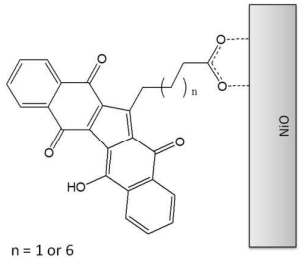

Fig. 8. Representation of KuQnCO$_2$H anchored on NiO.

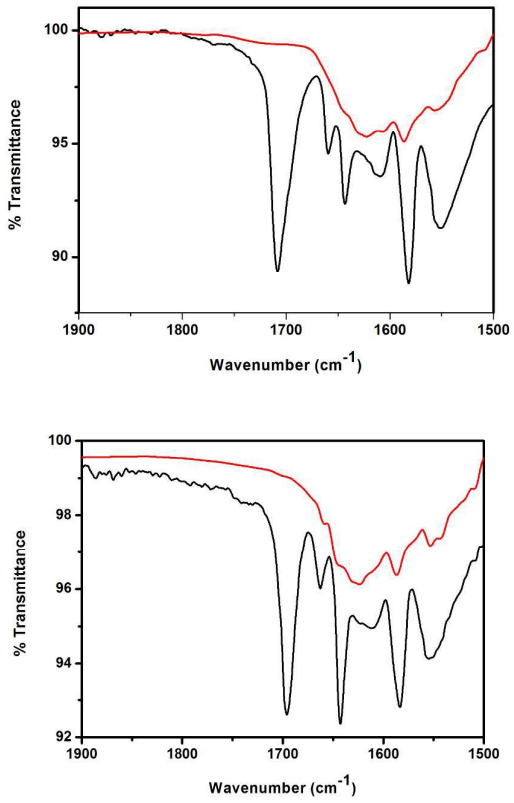

Fig. 9. FT-IR spectra of KuQ3CO$_2$H (on the top) and KuQ8CO$_2$H (on the bottom) pure (black line) and on NiO (red line). NiO background has been subtracted from each spectrum.

View Article Online
DOI: 10.1039/C6NJ03466G

KuQs-sensitized *p*-DSSC

The KuQ3CO$_2$H and KuQ8CO$_2$H sensitized NiO electrodes have been employed as photocathodes in *p*-type DSSCs. The performances obtained with KuQs-sensitized DSSC have been compared with the one of EryB-sensitized DSSC. The *JV* curves and the relative photoelectrochemical parameters are reported in Figure 10 and Table 2, respectively. Open circuit potential (V_{OC}) values were very similar one to each other. The higher value of 98.7 mV has been measured for KuQ8CO$_2$H. At a structural level, the higher V_{OC} measured in the KuQ8CO$_2$H sensitized cell is consistent with the longer side chain that produces a strong effect of electrode passivation, thus reducing recombination phenomena.

Fill Factor (FF) values were quite similar for all the dyes. The most important difference has been observed for the short circuit current density (J_{SC}): in fact EryB and KuQ3CO$_2$H devices exceeded the value of 0.7 mA/cm^2. This is probably due to the higher dye loading if compared with KuQ8CO$_2$H. Even though Ery B and KuQ3CO$_2$H induced the same current density in the *p*-DSSC, the mechanisms of charge transfer appeared different. In fact, for Ery B sensitizer, as for other well known dyes, the photoproduced electron is transferred from the dye to the semiconductor surface through a conjugated system of electronically conjugated bonds.

On the contrary, by using KuQuinones dyes, such mechanism is not practicable. In fact, the anchoring group is linked to the acceptor unit through a fully saturated alkyl chain, therefore an alternative but equally efficient mechanism occurs. Hence, the quantomechanic effect of tunneling is expected.

In particular, when the alkyl chain is sufficiently short, as for KuQ3CO$_2$H dye, the electron acceptor unit of the dye is quite close to the NiO surface, thus making the *ET* from the dye to the NiO surface a feasible event.

Clearly, the quantum yield of such phenomenon is strongly dependent on the length of the alkyl chain: a shorter chain should imply higher quantum yields. Interestingly, current intensities of KuQ3CO$_2$H and KuQ8CO$_2$H were not as different as we could expect, although the latter one contains a longer alkyl side chain (5 sp^3 carbon atoms). In this context, it should be considered that the long side chain may be able to bend on itself: in this condition the KuQ core of KuQ8CO$_2$H may be approximately at the same distance of KuQ3CO$_2$H from the oxide surface with consequent generation of devices with similar efficiency. This explanation should be considered as tentative and some different experiments have to be performed in order to properly prove it; nevertheless it is strongly consistent with the reported results (see IR analysis).

Table 2. Key parameters deducted by the *JV* curves. Errors have been calculated on the average of 3 similar devices.

Dye	V_{OC} (mV)	J_{SC} (mA/cm^2)	FF (%)	η (%)
Ery B	90.6±0.8	0.74±0.06	35.0±0.6	0.023±0.001
KuQ3CO$_2$H	92.2±0.9	0.74±0.04	35.9±0.3	0.025±0.002
KuQ8CO$_2$H	99.0±1.0	0.63±0.04	36.6±0.3	0.022±0.001

Parameters obtained by *JV* curves were in agreement with those obtained by IPCE (Incident photon-to-current conversion efficiency) analysis (Fig. 11).

From figure 11 two different contributions can be highlighted: an intense peak (about 8-10%) between 320 and 450 nm, which is due to the NiO bare (mostly from Ni^{3+} centers) and a second signal that is due to the photoexcitation of the dyes at wavelengths higher than 500 nm. The latter peak is specific of the dye: as already reported in trasmittance spectra, Ery B peak was quite sharp whereas the KuQs ones were broad.

It is mandatory to stress how both peaks contribute to the overall cell efficiency. Interestingly, KuQ8CO$_2$H and KuQ3CO$_2$H showed very similar IPCE spectra, although the latter has a higher overall efficiency than KuQ8CO$_2$H. Furthermore, from IPCE spectra it is evident that the photoelectrochemical contribution of NiO became lower upon sensitization. In particular, KuQ8CO$_2$H showed higher APCE (Absorbed Photon-to-current Conversion Efficiency, not shown) but lower LHE (Light Harvesting Efficiency) if compared with KuQ3CO$_2$H.

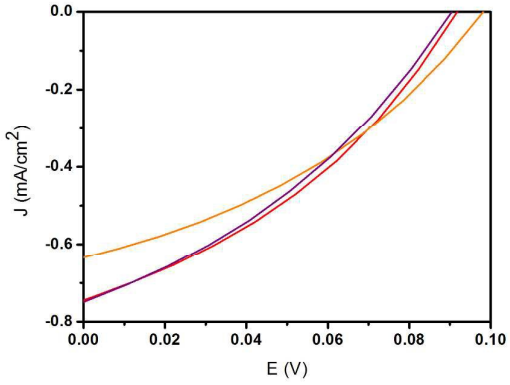

Fig. 10. *JV* curves for complete *p*-DSSC sensitized with: EryB (purple line), KuQ3CO$_2$H (red line), KuQ8CO$_2$H (orange line).

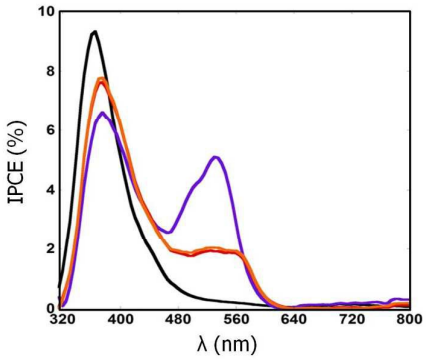

Fig. 11. IPCE spectra of complete p-DSSC sensitized with different dyes: EryB (purple line), KuQ3CO2H (red line), KuQ8CO2H (orange line). In black has been reported the IPCE spectra of a undyed NiO-based device.

View Article Online
DOI: 10.1039/C6NJ03466G

This is probably due to the decrease of the Ni^{3+} centers that constitute the preferential sites of dye anchoring. The more pronounced decrease of the IPCE peak typical of NiO in KuQs spectra with respect to ERY B system is due to the fact that KuQs absorb light also between 300 and 400 nm in a non effective way for charge photoexcitation.

Moreover, control experiments have been carried out in the absence of light (Table 3 and Fig. 12) to evaluate the dark current. Under the adopted experimental conditions, the dark cathodic current was probably due to the dark reduction of triiodide to iodide, $I_3^- + 2e^- \rightarrow 3I^-$ at the NiO/dye/electrolyte interface and, eventually, at the FTO/electrolyte interface. The latter interface can participate in the electrochemical process if the NiO layer is not compact, thus not preventing the effect of shunting between FTO substrate and the electrolyte.[14,65]

In the present work, the deposition of a compact NiO layer for the prevention of shunting was not considered. Therefore, shunting can occur at the TCO/electrolyte interface if the first layer of nanoporous NiO (which is in direct contact with FTO) does not uniformly cover the transparent conductive coating.

This evidence may imply that part of the surface charge in the cathode of the sensitized cell can be generated either from a process of dark charge transfer between dye and NiO substrate or from an anion physisorption process, depending on the nature of the anchored sensitizer and on its surface concentration.

With respect to NiO bare, all the sensitized devices showed higher values of open circuit potential and larger current densities. Moreover, the largest values of potential were combined to the largest values of current density.

Table 3. Parameters obtained by the dark *JV* measurement.

Dye	NiO bare	Ery B	$KuQ3CO_2H$	$KuQ8CO_2H$
J_{SC} (mA/cm^2)	-0.007	-0.015	-0.008	-0.012
V_{oc} (mV)	0.048	0.076	0.051	0.064

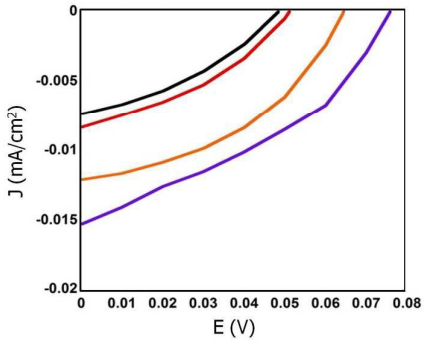

Fig. 12. JV curves in the dark: NiO bare (black line), EryB (purple line), KuQ3CO2H (red line), KuQ8CO2H (orange line).

Interestingly, all *JV* curves showed similar slopes to the ones generated by pristine NiO. This finding led us to conclude that these dyes do not have a catalytic or quenching effect for NiO towards the dark reduction process $I_3^- + 2e^- \rightarrow 3I^-$. Thus, triiodide reduction occurs exclusively on NiO bare (and eventually from the exposed FTO) when no light is absorbed by the KuQs sensitized system.[46,66]

Conclusions

In this work, new KuQuinone derivatives having a carboxylic acid terminal group and differing in side chain length have been synthesized. Desired products have been obtained in good yields if compared with the previously reported synthetic procedures of differently substituted KuQs.[54] Due to their favorable spectroscopic properties, such as the intense absorption in the visible region of the spectrum and their calculated HOMO-LUMO energy levels, these organic compounds have been anchored on NiO to test their application as sensitizers in *p*-type DSSCs. Results highlighted that KuQuinones-sensitized cells showed a better photoelectrochemical performance than Ery B, a conventional benchmark dye-sensitizer for *p*-DSSCs. In particular, fill factor (FF) values were analogous for all the tested dyes, while current density values (J_{SC}) were similar for Ery B and $KuQ3CO_2H$. The latter sensitizer was loaded in larger amount with respect to $KuQ8CO_2H$, because of the smaller chain length. Despite the lack of electronic conjugation between the anchoring unit and the light-absorbing unit, the photoinduced charge transfer occurred through space and not through the conjugated linker, as expectable. These findings indicate that the new dyes here proposed are particularly interesting photosensitizers for NiO-based *p*-type DSSCs. Obviously, the synthesis of novel KuQuinone derivatives possessing the light absorbing pentacyclic unit directly linked with the anchoring group through a conjugated π-linker is expected to improve the effectiveness of the charge transfer processes with consequent beneficial effects on the overall performance of the device.

Experimental

Materials

All commercial reagents and solvents were purchased from Sigma-Aldrich or Fluka, at the highest degree of purity available and were used without any further purification. Anhydrous terpineol was used as a mixture of enantiomers. FTO-covered glass panel (item no. TCO227) was purchased from Solaronix, HSE commercial liquid electrolyte from Dyesol and the liquid resin (3035B) from Threebond.

Instrumentation

^{1}H NMR spectra were recorded with a Bruker Avance 300 MHz instrument, using $CDCl_3$ as solvent. HRMS analyses have been

View Article Online
DOI: 10.1039/C6NJ03466G

performed with LCQ Duo instrument (ThermoQuest, San Jose, CA, USA). Gas chromatographic analyses were carried out with a Varian 3900 instrument equipped with a FID 1770 detector and a 30 m Supelco SPB-5 column (0.25 mm diameter and 0.25 µm internal film). UV-visible absorption spectra were recorded on a Shimadzu 2450 spectrometer equipped with the UV Probe 2.34 program. The thickness (*l*) of the NiO film was estimated with a Dektat 150® profilometer from Veeco. The imaging of the surface morphology of mesoporous NiO was realized with an Auriga Zeiss instrument. The measurements of optical transmittance of the sensitized NiO electrodes were made with a double ray spectrometer (UV-2550 by Shimazdu). The cyclic voltammetries of the solutions of KuQs were recorded with a Palmsens potentiostat. A standard calomel electrode (SCE) was used as the reference electrode, a platinum wire as counter electrode and a platinum disk as the working electrode. Measurements have been performed in a 0.1 M solution of tetrabutylammonium perchlorate (TBAP, crystallized from ethyl acetate) in anhydrous dichloromethane at a scan rate of 100 mV/s. ATR-FTIR spectra have been obtained as sum of 128 scans at a resolution of 4 cm^{-1} using a Thermonicolet iS50-FTIR instrument. Photoelectrochemical characterizations were carried out using the solar simulator Solar Test 1200 KHS (class B) at 1000 W/m^{-2} with artificial solar spectrum AM 1.5 G. The IPCE curves were recorded using a computer controlled set-up consisting of a Xe lamp (Mod.70612, Newport) coupled to a monochromator (Cornerstone 130 from Newport) and a Keithley 2420 as light-source meter.

NiO paste preparation and deposition

The preparation of the NiO paste constituting the precursor for the screen-printing step, has been carried out following a previously reported procedure.[38] The aspect of innovation in the modified method adopted in this work is the use of preformed NiO nanospheres (max diameter=50 nm) instead of common NiO chemical precursors, such as $NiCl_2$ or $Ni(OH)_2$, which generally render the purification and sintering processes much more laborious.[17]

The obtained paste was spread over a FTO-covered glass panel previously cleaned by an ultrasonic bath in acetone for 10 minutes and in ethanol for 10 minutes. The paste was spread via screen-printing through a 90.48 T mesh screen on dried FTO/glass panels. After a pre-drying period of 15 minutes at 100°C in oven (WHT 5/120 from Welland), the temperature was gradually increased with a ramp of 15°C/min up to 450 °C. The screen-printed slurry of NiO nanoparticles was kept at the highest temperature for 30 minutes to complete the sintering. After this period, the resulting mesoporous film of NiO was cooled down to room temperature and a 2 µm thick film of NiO was obtained. Furthermore, at the adopted temperature of sintering, the binders were completely combusted, so they were removed as volatile products of thermolysis from the oxide layer. The resulting oxide has generally non stoichiometric features and a more appropriate formula for describing it is NiO_x.

Synthesis

General synthetic procedure. KuQuinone derivatives have been synthesized according to a previously reported literature procedure.[54] Glassware was dried under nitrogen before the use. In a typical experiment, 1 g (5.75 mmol) of 2-hydroxy-1,4-naphthoquinone and 2.5 g (8 mmol) of anhydrous Cs_2CO_3 were insert in a 50 ml round flask. 12 mmol of the properly substituted alkyl bromide were added, together with 62 mg (0.33 mmol) of sublimated ferrocene. Reagents were dissolved in 22 ml of spectrophotometric grade DMSO (kept overnight over anhydrous K_2CO_3 prior to use). The mixture was kept under stirring at 114°C for 41 hours, then diluted with 100 ml of dichloromethane and filtered. The filtrate was then washed with water or brine (2× 500 ml), dried over anhydrous Na_2SO_4 and filtered. Solvent was removed under reduced pressure and the brown powder obtained was than purified by chromatography. The isolated purple compound was then repeatedly crystallized from dichloromethane–pentane.

1-methylKuQuinone ($KuQCH_3$). The reaction was carried out according to the reported general procedure, using 1-bromopropane as alkyl bromide reagent. The brown powder obtained was purified with a chromatography column on SiO_2, using CH_2Cl_2 as eluent. 60 mg (0.17 mmol) of $KuQCH_3$ as a purple powder have been obtained (6.1 % yield). ^{1}H NMR in $CDCl_3$: δ 18.11 (s, 1H), δ 8.30–8.25 (m, 4H), δ 7.80–7.74 (m, 4H), δ 2.98 (s, 3H). HRMS (ESI-) *m/z*: $[M-H]^-$ calcd. for $C_{22}H_{11}O_4$ 339.0657; found 339.0642.

Ethyl 11-bromoundecanoate. 6 g of 11-bromoundecanoic acid (23 mmol) were dissolved in 200 ml of absolute ethanol, with the addition of catalytic amount of 37% HCl solution. The reaction mixture was kept under stirring at 40°C and checked by GC analysis. Subsequently, it was diluted with 300 ml of water and extracted with diethyl ether (3 × 250 ml). Organic phase was dried over anhydrous Na_2SO_4 and filtered. The solvent was evaporated under reduced pressure and a pale yellow liquid has been obtained (6.1 g, 10 mmol, 90% yield). ^{1}H NMR in $CDCl_3$: δ 4.18-4.10 (q, 2H), δ 3.45-3.40 (t, 2H), δ 2.34-2.28 (t, 2H), δ 1.91-1.82 (m, 2H), δ 1.68-1.60 (m, 4H), δ 1.46-1.25 (m + t, 13H).

Ethyl 6-bromohexanoate. 4.3 g of 6-bromohexanoic acid 97% (22 mmol) were dissolved in 200 ml of absolute ethanol, and 1 ml of 37% HCl solution was added. The reaction mixture was kept under stirring at 40°C and checked by GC analysis. Afterwards, it was concentrated, diluted with Et_2O and extracted with water (2 × 200 ml). Organic phase was dried over Na_2SO_4 and filtered and the solvent was evaporated under reduced pressure to give a pale yellow liquid (4.4 g, 20 mmol, 90% yield). ^{1}H NMR in $CDCl_3$: δ 4.18-4.10 (q, 2H), δ 3.45-3.40 (t, 2H), δ 2.35-2.30 (t, 2H), δ 1.94-1.84 (m, 2H), δ 1.72-1.62 (m, 2H), δ 1.54-1.43 (m, 2H), δ 1.25-1.24 (t, 3H).

1-(8-ethoxycarbonyloctyl)KuQuinone ($KuQ8CO_2Et$). The reaction was carried out with ethyl 11-bromoundecanoate as alkyl bromide and according to the general procedure previously described. The brown powder was purified by *plug* chromatography (SiO_2, eluent CH_2Cl_2); the isolated purple product (184 mg, 0.36 mmol, 13% yield) was then crystallized

View Article Online
DOI: 10.1039/C6NJ03466G

from dichloromethane-hexane and washed with pentane. ^{1}H NMR in $CDCl_3$: δ 18.16 (s, 1H), δ 8.29–8.25 (m, 4H), δ 7.84–7.71 (m, 4H), δ 4.17–4.10 (q, 2H), δ 3.49–3.44 (t, 2H), δ 2.32–2.27 (t, 2H), δ 1.68–1.36 (m, 12H + H_2O), δ 1.29–1.24 (t, 3H). HRMS (ESI-) *m/z*: $[M-H]^-$ calcd. for $C_{32}H_{30}O_6$ 509.19696; found 509.19686.

1-(8-carboxyloctyl)KuQuinone (KuQ8CO2H). 49 mg of $KuQ8CO_2Et$ (0.096 mmol) were dissolved in 8 ml of THF. Afterwards, 2 ml of NaOH 25% in MeOH were added and the system was kept under stirring for one hour and checked by TLC analysis (SiO_2, eluent CH_2Cl_2). Reaction mixture was diluted with 100 ml of NH_4Cl 10%, neutralized with HCl 1 M and extracted with CH_2Cl_2. Organic phase was dried over Na_2SO_4, filtered and the solvent was removed under reduced pressure. $KuQ8CO_2H$ has been obtained as a purple powder (44 mg, 0.090 mmol, 95% yield). Due to the low solubility of the product ^{1}H NMR analysis was not practicable. HRMS (ESI-) *m/z*: $[M-H]^-$ calcd. for $C_{30}H_{26}O_6$ 481.1657; found 481.1728.

1-(3-ethoxycarbonylpropyl)KuQuinone (KuQ3CO2Et). The reaction was carried out using ethyl 6-bromohexanoate as alkyl bromide and according to the general procedure. The product has been purified by *plug* chromatography (SiO_2, eluent CH_2Cl_2); the isolated purple powder (173 mg, 0.40 mmol, 14% yield) was crystallized from dichloromethane-hexane and then washed with pentane. ^{1}H NMR in $CDCl_3$: δ 18.20 (s, 1H), δ 8.27-8.22 (m, 4H), δ 7.79-7.71 (m, 4H), δ 4.15-4.11 (q, 2H), δ 3.53-3.50 (t, 2H), δ 2.50-2.47 (t, 2H), δ 2.09-2.04 (m, 2H), δ 1.25-1.23 (t, 3H). HRMS (ESI-) *m/z*: $[M-H]^-$ calcd for $C_{27}H_{20}O_6$ 439.1187; found 439.1207.

1-(3-carboxylpropyl)KuQuinone ($KuQ3CO_2H$). 45 mg of $KuQ3CO_2Et$ (0.10 mmol) were dissolved in 50 ml of THF. Afterwards, 5 ml of a saturated solution of NaOH in MeOH were added and the system was kept under stirring overnight and checked by TLC analysis (SiO_2, eluent CH_2Cl_2). After neutralization with 0.1 M HCl, a purple precipitate has been obtained. 39.2 mg of the product have been obtained as a purple powder (0.095 mmol, 95% yield). HRMS (ESI-) *m/z*: $[M-H]^-$ calcd. for $C_{25}H_{16}O_6$ 411.0874; found 411.0898.

Theoretical calculations

Computational calculations were performed using Gaussian 09 rev. A.02.[59] Geometry optimization was carried out using density functional theory (DFT) and B3LYP hybrid functional with 6-31G+dp basis set, while HOMO-LUMO energy levels have been calculated with 6-311G dp basis set in the vacuum.

Devices assembly

Platinized counter electrodes were prepared by screen printing platinum paste Ch01 from Chimet through a 100T mesh screen onto FTO-coated glass.[67] Sensitization of screen-printed NiO photocathodes was carried out through 16 hours dipping in a solution of the corresponding dye: $KuQCH_3$ (0.3 mM in toluene), $KuQ8CO_2H$ (0.3 mM in THF), $KuQ3CO_2H$ (0.2 mM in THF). THF was used as solvent to dissolve $KuQ8CO_2H$ and $KuQ3CO_2H$ dyes due to their very low solubility in other conventional organic solvents.

As a comparison, NiO photocathodes have been functionalized also with the commercially available dye Ery B, using 0.2 mM solution in ethanol. All screen-printed NiO samples were sensitized at room temperature for 16 hours and then washed with the same solvent used in the dipping phase. The screen-printed NiO photocathode and the platinized FTO counter electrode were assembled together in a sandwich configuration using Bynel® thermoplastic polymeric film having the double function of being spacer and sealant. After sandwiching the electrodes, the triiodide/iodide HSE commercial liquid electrolyte was injected inside the cell by *vacuum* backfilling technique. The hole for electrolyte injection was sealed with a liquid resin (3035B) which becomes a hard paste upon UV curing treatment. The photoactive area of the samples was 0.25 cm^2.

Devices Characterization

The relationship between the characteristic parameters of the diode-like *JV* curves is $\eta=[(J_{SC}*V_{OC})*FF]/I_{in}$ in which the term I_{in} indicates the intensity (in $W\cdot m^{-2}$) of the radiation incident on the electrochemical photoconversion device. The IPCE spectra directly provide the percentage of incident photons converted into electrons, at a given wavelength. IPCE (sometimes denominated external quantum efficiency, EQE) is defined as $IPCE(\lambda)=[J_{SC}(\lambda)/e]/\Phi_{in}(\lambda)]$ where *e* represents the elementary charge, and $\Phi_{in}(\lambda)$ the flux of photons with energy $h(c/\lambda)$ which impinge the unit surface of illuminated device per unit time (in photons $m^{-2}s^{-1}$). In the definition of photonic energy the symbols *h*, *c* and λ indicate the Planck's constant, the speed of light and the radiation wavelength, respectively. The defined concept of IPCE leads to the relationship $IPCE(\lambda)=LHE(\lambda)*\Phi_{inj}(\lambda)*\eta_{CC}=LHE(\lambda)*\Phi_{inj}(\lambda)*\Phi_{esc}(\lambda)*\eta_{tr}$,[40] where LHE(λ) is the light harvesting efficiency of the dye at a given wavelength λ, $\Phi_{inj}(\lambda)$ is the efficiency of charge injection from the excited dye to the semiconductor substrate at the wavelength of absorption λ (also called hole injection quantum yield), $\Phi_{esc}(\lambda)$ is the escape quantum yield, i.e. the probability that a photoinjected hole has to escape from direct recombination with the reduced dye (also Φ_{esc} is wavelength-dependent), η_{tr} is the probability the hole has to avoid all processes of recombination and reaches the current collector, and η_{CC} is the charge collection efficiency which refers to the efficiency of the transfer of the photoinjeted charge from the site of photogeneration localized at the semiconductor/dye interface, to the surface of the current collector (typically the semiconductor/TCO interface). The LHE(*λ*) is related to the absorbance A(λ) at a given wavelength (λ) of the dye-sensitizer in the anchored state by the relationship $LHE(\lambda)=1-10^{-A(\lambda)}$.

Acknowledgements

P.G. thanks the project "Ricerca Scientifica d'Ateneo 2015 from University of Rome Tor Vergata, SMART project" for financial support. D.D. acknowledges the financial support from the University of Rome "LA SAPIENZA" through the program Ateneo 2012 (Protocol No. C26A124AXX). Dr. Claudia Mazzuca

View Article Online
DOI: 10.1039/C6NJ03466G

and Dott. Benedetta Di Napoli are gratefully acknowledged for ATR-FTIR experiments and authors thank Dr. Fabio Matteocci for useful discussions and technical details.

Notes and references

1 T. Daeneke, Z. Yu, G.P. Lee, D. Fu, N.W. Duffy, S. Makuta, Y. Tachibana, L. Spiccia, A. Mishra, P. Bäuerle and U. Bach, *Adv. Energy Mater.*, 2015, **5**, 1401387.
2 L. Zhang, G. Boschloo, L. Hammarström and H. Tian, *Phys. Chem. Chem. Phys.*, 2016, **18**, 5080.
3 D. Dini, Y. Halpin, J. G. Vos and E. A. Gibson, *Coord. Chem. Rev.*, 2015, **304-305**, 179.
4 D. Dini, *Phys. Chem. Commun.*, 2016, **3**, 14.
5 L. Li, L. Duan, F. Wen, C. Li, M. Wang, A. Hagfeldt and L. Sun, *Chem. Commun.*, 2012, **48**, 988.
6 M. Halmann, *Nature*, 1978, **275**, 115.
7 T. Inoue, A. Fujishima, S. Konishi and K. Honda, *Nature*, 1979, **277**, 637.
8 E. E. Barton, D. M. Rampulla and A. B. Bocarsly, *J. Am. Chem. Soc.,* 2008, **130**, 6342.
9 I. R. Perera, T. Daeneke, S. Makuta, Z. Yu, Y. Tachibana, A. Mishra, P. Bäuerle, C. A. Ohlin, U. Bach and L. Spiccia, *Angew. Chem. Int. Ed.*, 2015, **54**, 1.
10 S. Powar, R. Bhargava, T. Daeneke, G. Götz, P. Bäuerle, T. Geiger, S. Kuster, F. A. Nüesch, L. Spiccia and U. Bach, *Electrochim. Acta*, 2015, **182**, 458.
11 J. He, H. Lindström, A. Hagfeldt and S. E. Lindquist, *Solar Energy Mater. Solar Cells*, 2000, **62**, 265.
12 A. Nakasa, H. Usami, S. Sumikura, S. Hasegawa, T. Koyama and E. Suzuki, *Chem. Lett.*, 2005, **34**, 500.
13 A. Nattestad, A. J. Mozer, M. K. R. Fischer, Y. B. Cheng, A. Mishra, P. Bäuerle and U. Bach, *Nature Mater.*, 2010, **9**, 31.
14 C. J. Wood, G. H. Summers and E. A. Gibson, *Chem. Commun.*, 2015, **51**, 3915.
15 C. H. Henry, *J. Appl. Phys.*, 1980, **51**, 4494.
16 J. Wood, G. H. Summers, C. A. Clark, N. Kaeffer, M. Braeutigam, L. R. Carbone, L. D'Amario, K. Fan, Y. Farre´, S. Narbey, F. Oswald, L. A. Stevens, C. D. J. Parmenter, M. W. Fay, A. La Torre, C. E. Snape, B. Dietzek, D. Dini, L. Hammarström, Y. Pellegrin, F. Odobel, L. Sun, V. Artero, and E. A. Gibson, *Phys. Chem. Chem. Phys.*, 2016, **18**, 10727.
17 L. Li, E. A. Gibson, P. Qin, G. Boschloo, M. Gorlov, A. Hagfeldt and L. Sun, *Adv. Mater.*, 2010, **22**, 1759.
18 S. Powar, Q. Wu, M. Weidelener, A. Nattestad, Z. Hu, A. Mishra, P. Bäuerle, L. Spiccia, Y.B. Cheng and U. Bach, *Energy Environ. Sci.*, 2012, **5**, 8896.
19 X. L. Zhang, F. Huang, A. Nattestad, K. Wang, D. Fu, A. Mishra, P. Bäuerle, U. Bach and Y. B. Cheng, *Chem. Commun.*, 2011, **47**, 4808.
20 M. Bonomo and D. Dini, *Energies*, 2016, **9**, 373/1-32.
21 M. Awais, M. Rahman, J. M. Don MacElroy, N. Coburn, D. Dini, J. G. Vos and D. P. Dowling, *Surf. Coat. Technol.*, 2010, **204**, 2729 and references therein**.**
22 A. Hagfeldt, G. Boschloo, L. Sun, L. Kloo and H. Pettersson, *Chem. Rev.*, 2010, **110**, 6595.
23 M. Awais, D. P. Dowling, F. Decker and D. Dini, *SpringerPlus*, 2015, **4**, 564/1-24.
24 M. Awais, D. P. Dowling, F. Decker and D. Dini, *Adv. Condens. Matter Phys.*, 2015, **2015**, 186375/1-18.
25 V. Novelli, M. Awais, D. P. Dowling and D. Dini, *Am. J. Anal. Chem.*, 2015, **6**, 176.
26 M. Bonomo, G. Naponiello, A. Di Carlo, D. Dini, *J. Mater. Sci. Nanotechnol.*, **2016**, *4*, 201/1-18.
27 M. Yu, G. Natu, Z. Ji and Y. Wu, *J. Phys. Chem. Lett.,* 2012, **3**, 1074.
28 M. Chitambar, Z. Wang, Y. Liu, A. Rockett and S. Maldonado, *J. Am. Chem. Soc.*, 2012, **134**, 10670.
29 F. Vera, R. Schrebler, E. Muñoz, C. Suarez, P. Cury, H. Gómez, R. Córdova, R. E. Marotti, E. A. Dalchiele, *Thin Solid Films*, 2005, **490**, 182.
30 A. Morandeira, G. Boschloo, A. Hagfeldt and L. Hammarström, *J. Phys. Chem. B*, 2005, **109**, 19403.
31 Y. Mizoguchi and S. Fujihara, *Electrochem. Solid State Lett.*, 2008, **11**, K78.
32 C. J. Flynn, E. B. E. Oh, S. M. McCullough, R. W. Call, C. L. Donley, R. Lopez and J. F. Cahoon, *J. Phys. Chem. C,* 2014, **118**, 14117.
33 A. Morandeira, G. Boschloo, A. Hagfeldt and L. Hammarström, *J. Phys. Chem. C*, 2008, **112**, 9530.
34 P. Qin, H. Zhu, T. Edvinsson, G. Boschloo, A. Hagfeldt and L. Sun, *J. Am. Chem. Soc.*, 2008, **130**, 8570.
35 P. Qin, J. Wilberg, E.A. Gibson, M. Linder, L. Li, T. Brinck, A. Hagfeldt, B. Albinsson and L. Sun, *J. Phys. Chem. C*, 2010, **114**, 4738.
36 X. L. Zhang, Z. Zhang, F. Huang, P. Bäuerle, U. Bach and Y. B. Cheng, *J. Mater. Chem.*, 2012, **22**, 7005.
37 D. Ameline, S. Diring, Y. Farre, Y. Pellegrin, G. Naponiello, E. Blart, B. Charrier, D. Dini, D. Jacquemin and F. Odobel, *RSC Adv.*, 2015, **5**, 85530.
38 M. Bonomo, N. Barbero, F. Matteocci, A. Di Carlo, C. Barolo and D. Dini, *J. Phys. Chem. C*, 2016, **120**, 16340.
39 J. Warnan, J. Gardner, L. Le Pleux, J. Petersson, Y. Pellegrin, E. Blart, L. Hammarström, F. Odobel, *J. Phys. Chem. C,* 2014, **118**, 103.
40 M. Borgström, E. Blart, G. Boschloo, E. Mukhtar, A. Hagfeldt, L. Hammarström and F. Odobel *J. Phys. Chem. B*, 2005, **109**, 22928.
41 J. F. Lefebvre, X. Z. Sun, J. A. Calladine, M. W. George and E. A. Gibson, *Chem. Commun.*, 2014, **50**, 5258.
42 Z. Liu, W. Li, S. Topa, X. Xu, X. Zeng, Z. Zhao, M. Wang, W. Chen, F. Wang, Y. B. Cheng and H. He, *ACS Appl. Mater. Interfaces*, 2014, **6**, 10614.
43 F. Wu, S. Zhao, C. Zhong, Q. Song and L. Zhu, *RSC Adv.*, 2015, **5**, 93652.
44 Y. Farré, L. Zhang, Y. Pellegrin, A. Planchat, E. Blart, M. Boujtita, L. Hammarström, D. Jacquemin and F. Odobel, *J. Phys. Chem. C*, 2016, **120**, 7923.
45 Y. Pellegrin, L. Le Pleux, E. Blart, A. Renaud, B. Chavillon, N. Szuwarski, M. Boujtita, L. Cario, S. Jobic, D. Jacquemin and F. Odobel, *J. Photochem. Photobio. A*, 2011, **219**, 235.
46 S. Sheehan, G. Naponiello, F. Odobel, D. P. Dowling, A. Di Carlo and D. Dini, *J. Solid State Electrochem.*, 2015, **19**, 975.
47 Z. Ji and Y. Wu, *J. Phys. Chem. C,* 2013, **117**, 18315.
48 L. D'Amario, L. J. Antila, B. Pettersson Rimgard, G. Boschloo and L. Hammarström, *J. Phys. Chem. Lett.,* 2015, **6**, 779.
49 L. Zhang and J. M. Cole, *ACS Appl. Mater. Interfaces*, 2015, **7**, 3427.
50 Q. H. Yao, F. S. Meng, F. Y. Li, H. Tian and C. H. Huang, *J. Mater. Chem*., 2003, **13**, 1048.
51 Y. Ooyama, Y. Shimada, Y. Kagawa, Y. Yamada, I. Imae, K. Komaguchi and Y. Harima, *Tetrahedron Lett*., 2007, **48**, 9167.
52 Y. Hao, X. Yang, J. Cong, H. Tian, A. Hagfeldt and L. Sun, *Chem. Comm*., 2009, 4031.
53 Y. Hao, C. J. Wood, C. A. Clark, J. A. Calladine, R. Horvath, M. W. D. Hanson-Heine, X. Z. Sun, I. P. Clark, M. Towrie, M. W. George, X. Yang, L. Sun and E. A. Gibson, *Dalton Trans*., 2016, **45**, 7708.
54 A. Coletti, S. Lentini, V. Conte, B. Floris, O. Bortolini, F. Sforza, F. Grepioni and P. Galloni, *J. Org. Chem.*, 2012, **77**, 6873.
55 F. Sabuzi, V. Armuzza, V. Conte, B. Floris, M. Venanzi, P. Galloni and E. Gatto, *J. Mater. Chem. C*, 2016, **4**, 622.
56 M. Awais, E. Gibson, J. G. Vos, D. P. Dowling, A. Hagfeldt and D. Dini, *ChemElectroChem*, 2014, **1**, 384.

View Article Online
DOI: 10.1039/C6NJ03466G

57 S. N. Dighe, R. V. Bhattad, R. R. Kulkarni, K. S. Jain and K. V. Srinivasan, *Synth. Commun*., 2010, **40**, 3522.
58 R. Giovannetti, The Use of Spectrophotometry UV-Vis for the Study of Porphyrins, Macro To Nano Spectroscopy, Dr. Jamal Uddin (Ed.), 2012.
59 M. J. Frisch, G. W. Trucks, H. B. Schlegel, G. E. Scuseria, M. A. Robb, J. R. Cheeseman, G. Scalmani, V. Barone, B. Mennucci, G. A. Petersson, H. Nakatsuji, M. Caricato, X. Li, H. P. Hratchian, A. F. Izmaylov, J. Bloino, G. Zheng, J. L. Sonnenberg, M. Hada, M. Ehara, K. Toyota, R. Fukuda, J. Hasegawa, M. Ishida, T. Nakajima, Y. Honda, O. Kitao, H. Nakai, T. Vreven, J. A. Montgomery Jr., J. E. Peralta, F. Ogliaro, M. Bearpark, J. J. Heyd, E. Brothers, K. N. Kudin, V. N. Staroverov, R. Kobayashi, J. Normand, K. Raghavachari, A. Rendell, J. C. Burant, S. S. Iyengar, J. Tomasi, M. Cossi, N. Rega, J. M. Millam, M. Klene, J. E. Knox, J. B. Cross, V. Bakken, C. Adamo, J. Jaramillo, R. Gomperts, R. E. Stratmann, O. Yazyev, A. J. Austin, R. Cammi, C. Pomelli, J. W. Ochterski, R. L. Martin, K. Morokuma, V. G. Zakrzewski, G. A. Voth, P. Salvador, J. J. Dannenberg, S. Dapprich, A. D. Daniels, O. Farkas, J. B. Foresman, J. V. Ortiz, J. Cioslowski, D. J. Fox, Gaussian 09, Revision A.02, Gaussian, Inc., Wallingford CT, 2009.
60 See as examples: a) M. Pastore, S. Fantacci and F. De Angelis, *J. Phys. Chem. C,* 2013, **117**, 3685; b) L. Leonat, G. Sbârcea and I. V. Brânzoi, *U.P.B. Sci. Bull. B*, 2013, **75**, 111; c) A. Georgiev, E. Bubev, D. Dimov, D. Yancheva, I. Zhivkov, J. Krajčovič, M. Vala, M. Weiter and M. Machkova, *Spectrochim. Acta A*, 2017, **175**, 76.
61 D. Sęk, M. Siwy, J. G. Małecki, S. Kotowicz, S. Golba, E. M. Nowak, J. Sanetra and E. Schab-Balcerzak, *Spectrochim. Acta A*, 2017, **175**, 168.
62 M. Bonomo, G. Naponiello, I. Venditti, V. Zardetto, A. Di Carlo and D. Dini, *J. Electrochem. Soc*., 2017, **164**, H137.
63 A. Ishii and T. Miyasaka, *Chem. Commun*., 2012, **48**, 9900.
64 J. Y. Park, B. Y. Jang, C. H. Lee, H. J. Yun and J. H. Kim, *RSC Adv*., 2014, **4**, 61248.
65 F. Fabregat-Santiago, J. Bisquert, E. Palomares, L. Otero, D. Kuang, S. M. Zakeeruddin, and M. Grätzel, *J. Phys. Chem. C*, 2007, **111**, 6550.
66 M. Bonomo, D. Dini and A. G. Marrani, *Langmuir*, 2016, **32**, 11540.
67 F. De Rossi, L. Di Gaspare, A. Reale, A. Di Carlo and T. M. Brown, *J. Mater. Chem. A*, 2013, **1**, 12941.

View Article Online
DOI: 10.1039/C6NJ03466G

KuQuinones have been used for the first time as dyes in NiO-based *p*-type DSSCs.